2 December 1994

ELSEVIER

Chemical Physics Letters 230 (1994) 463–472

CHEMICAL PHYSICS LETTERS

Density matrix description of laser-induced hot electron mediated photodesorption of NO from Pt(111)

Peter Saalfrank [a], Roi Baer [b], Ronnie Kosloff [b]

[a] *Institut für Physikalische und Theoretische Chemie, Freie Universität Berlin, Takustraße 3, D-14195 Berlin, Germany*

[b] *Department of Physical Chemistry and the Fritz-Haber Research Center for Molecular Dynamics, The Hebrew University, Jerusalem 91904, Israel*

Received 25 August 1994

Abstract

Based on the numerical solution of the Liouville–von Neumann equation for dissipative systems, the photodesorption dynamics of NO/Pt(111) are studied. Dissipative terms are used to describe the quenching of electronically excited states on the metal, electronic dephasing and the indirect (hot-electron mediated) excitation processes in the DIMET and DIET limits. Norm and energy flow, desorption probabilities and density time-of-flight spectra are computed.

1. Introduction

Photochemistry at adsorbate covered surfaces is a rapidly developing field of research. Pulsed laser sources through the pump and probe technique have added new insight into the field. Besides the spectroscopic characterization of static or dynamic properties of the adsorbate/substrate system, lasers can be also used used to control, perhaps selectively, chemical reactions at surfaces.

In the most simple application, the laser light heats the surface which then induces a phonon-driven chemistry. More interesting, and the focus of the present study are the truly photochemical events, where usually more than one electronic surface participates. A prominent example is the UV/VIS laser-induced desorption of small molecules from solid substrates. In the simplest, one-dimensional, two-state models due to Menzel, Gomer and Redhead (MGR) [1], and Antoniewicz [2], adsorbate-excited electronic surfaces are postulated to asists the desorption process. More refined models take the continuum nature of the electronic excitation spectra of solids into account [3]. In the case of insulators, the transition from a bound ground state surface to a repulsive (MGR) or bound (Antoniewicz) one proceeds via *direct* excitation of the molecule–surface bond (see, for instance, Ref. [4].)

For most metals, on the other hand, it is assumed that the transition is *indirect*, i.e. mediated by 'hot electrons' which have been created following absorption of the laser field by the metal (conduction) electrons. The hot electrons have an enhanced probability of resonantly tunneling through a barrier separating the solid from the adsorbate. A negative ion resonance is formed, which decays rapidly, within a few femtoseconds for metals, due to quenching. Depending on whether during this short lifetime enough kinetic (MGR) or potential energy (Antoniewicz) has been gained to overcome the binding energy on the lower (neutral) surface, the particle may desorb or will be retrapped in the ground state well.

For the indirect excitation step taking place in metals, one may further distinguish between two experi-

SSDI 0009-2614(94)01182-6

mentally realizable limits, namely desorption induced by electronic transitions (DIET) [5] (realized, for instance for NO/Pt(111) [6]), and desorption induced by multiple electronic transitions DIMET [7] (realized, for instance for NO/Pd(111)). DIET occurs in the continuous wave (cw) limit of irradiation bl in practice one uses nanosecond laser pulses. Hot carriers are characterized here by a time-independent non-Boltzmann energy distribution created by the pulse and so-called hot electron cascades [8]. In the DIMET limit on the other hand, ultrashort, femtosecond laser pulses are used [7]. This way temporarily high concentrations of electron-hole pairs are achieved which rapidly thermalize, giving rise to a time-peaked electronic temperature profile $T_e(t)$ with thousands of kelvins peak temperature. At the same time the phonon temperature increases only slowly and moderately. During the high-T_e period multiple transitions between the electronic surfaces can occur. The different excitation limits cause different experimental outcomes. For instance, the desorption probability is usually lower for DIET than for DIMET, and scales differently with the laser fluence (linear for DIET, non-linear for DIMET).

This Letter is intended to study dynamical details of the desorption of a small molecule, NO, from a metal, Pt(111), both in the DIET and DIMET limits. In contrast to previous time-dependent studies on this system, which used semiclassical [9] or quantum wave packets [10] to describe the desorption process (and which considered only the DIET experiment), we will numerically solve the Liouville–von Neumann equation [11] by propagating density matrices rather than wavefunctions in time. The density matrix description has the advantages of (i) naturally being applicable to thermal (mixed) states, and (ii) to allow for an easy inclusion of energy- and phase-exchange between a small 'system' (the adsorbate–substrate complex) and a 'bath' (the solid). These exchange terms enter the quantum mechanical equations of motion in a phenomenological manner. Consequently one does not gain full insight into the microscopic events underlying the excitation and the deexcitation processes, but within a few reasonable assumptions it is possible to extract the essential dynamical features in the theoretically most consistent way.

2. Model selection and methodology

In our treatment of the photostimulated desorption of NO from Pt(111) we use a one-dimensional two-surface model as put forward by Gadzuk [9]. For the ground state potential energy surface (PES) we write

$$V_g(z)=D\{1-\exp[-\alpha(z-z_0)]\}^2, \tag{1}$$

with z being the distance between the surface and the molecule. The Morse parameters, well depth $D=1.08$ eV and exponent $\alpha=1.708\ a_0^{-1}$, are chosen to give best fits to experimental data. The equilibrium distance z_0 is unknown and treated parametrically. For the excited state $V_e(z)$ modelling the negative ion resonance, the following parametrization is used [12]:

$$V_e(z)=D\{1-\exp[-\alpha(z-z_0+\Delta z)]\}^2 - \frac{(\delta e)^2}{4(z-z_{im})}+\epsilon . \tag{2}$$

Here, the last term accounts for the proper asymptotics ($\lim_{z\to\infty}(V_e(z)-V_g(z))=\epsilon=\phi-\mathrm{EA}$, with ϕ, denoting the work function of Pt(111) and EA the electron affinity of NO). The second term accounts for the stabilization of $V_e(z)$ due to the formation of an image charge following charge transfer to the adsorbate. ($z_{im}\equiv 0$ is the image plane, δe the fraction of charge transferred.) Finally, Δz allows for the possibility of strengthening ($\Delta z>0$) the molecule-surface bond in the excited state, due to the occupation of NO–metal bonding orbitals during the formation of the negative ion resonance. The results shown below are for the parameters $z_0=1.5$ Å, $\delta e=1e$, $\Delta z=0.20\ a_0$ and $\epsilon=5$ eV.

The propagation in time of the density operator $\boldsymbol{\rho}$ is governed by the Liouville–von Neumann equation, which for our two-state problem can be written as [13]:

$$\frac{\partial}{\partial t}\begin{pmatrix}\rho_e & \rho_i\\ \rho_i^+ & \rho_g\end{pmatrix}=-\frac{i}{\hbar}\left[\begin{pmatrix}H_e & V_{eg}\\ V_{eg}^* & H_g\end{pmatrix},\begin{pmatrix}\rho_e & \rho_i\\ \rho_i^+ & \rho_g\end{pmatrix}\right] + \frac{\partial}{\partial t}\begin{pmatrix}\rho_e & \rho_i\\ \rho_i^+ & \rho_g\end{pmatrix}_{diss}. \tag{3}$$

Eq. (3) consists of a Hamiltonian part (the commutator, [,]) which describes the evolution of the 'sys-

tem' alone (the adsorbate–substrate complex), and a dissipative part ('diss'), describing externally induced exchange of energy, norm or phase within the system or between the system and a 'bath' (the rest of the solid and/or neglected system-degrees of freedom). It has been shown by Lindblad [14] that the dissipative part can be cast in the form

$$\frac{\partial}{\partial t}\boldsymbol{\rho}_{\mathrm{diss}} = \sum_j \gamma_j (\mathbf{W}_j \boldsymbol{\rho} \mathbf{W}_j^{+} - \tfrac{1}{2}[\mathbf{W}_j^{+}\mathbf{W}_j, \boldsymbol{\rho}]_+) , \qquad (4)$$

with γ_j being a characteristic rate describing the energy, norm or phase transport in dissipative channel j, and the $\mathbf{W}_j$ being, in our two-state case, 2×2-matrix operators from the Hilbert space of the open system. These operators determine, roughly speaking, in which mode energy, norm, or phase flows. Further, $[\ ,\ ]_+$ in Eq. (4) stands for an anticommutator.

In the present model, the diagonal elements of the Hamiltonian matrix operator are

$$\boldsymbol{H}_l = -\frac{\hbar^2}{2\mu}\frac{\partial^2}{\partial z^2} + V_l(z) \qquad (5)$$

(with l=e, g), and Hamiltonian coupling V_{eg} is assumed to be of the form

$$V_{\mathrm{eg}}(z,t) = -\mu_{\mathrm{eg}}(z)\epsilon(t) + A\exp[-(z-z_{\mathrm{c}})^2/b] . \qquad (6)$$

Here, the first term accounts for a possible *direct* excitation of the molecule–surface bond ($\mu_{\mathrm{eg}}(z)$ is a transition dipole function, $\epsilon(t)$ the time-dependent laser field), and the second one for non-adiabatic (inter-surface, non-Born–Oppenheimer) coupling, modelled by a Gaussian centered around the crossing point z_{c} of the two *diabatic* potentials V_{g} and V_{e}. Since for the present system only indirect excitation is of importance, we take $\mu_{\mathrm{eg}}=0$. The non-adiabatic strength and width parameters A and b were varied in reasonable typical gas phase ranges.

Further, the following dissipative terms are included. The first process to simulate is the *quenching* of the molecular excited state (surface 'e') due to coupling of the center-of-mass motion to electronic degrees of freedom of the metal substrate. This ultrafast radiationless decay transfers norm and energy in the direction e→g and is modelled with the help of the Hilbert space operator $\mathbf{W}_1$,

$$\mathbf{W}_1 = \mathbf{S}_- \equiv \begin{pmatrix} 0 & 0 \\ 1 & 0 \end{pmatrix} \qquad (7)$$

and a characteristic quenching rate γ_1. With this choice of $\mathbf{W}_1$ it follows from Eqs. (3) and (4) that

$$\frac{\partial}{\partial t}\begin{pmatrix} \rho_{\mathrm{e}} & \rho_{\mathrm{i}} \\ \rho_{\mathrm{i}}^{+} & \rho_{\mathrm{g}} \end{pmatrix}_{\mathrm{diss},1} = \gamma_1 \begin{pmatrix} -\rho_{\mathrm{e}} & -\tfrac{1}{2}\rho_{\mathrm{i}} \\ -\tfrac{1}{2}\rho_{\mathrm{i}}^{+} & \rho_{\mathrm{e}} \end{pmatrix} . \qquad (8)$$

Eq. (8) manifestly shows how the norm is transferred from the upper to the lower surface, and that the 'coherencies' ρ_{i} and ρ_{i}^{+} decay only half as fast as the diagonal density exchange proceeds.

The second dissipative channel considered is *electronic dephasing*, i.e. the loss of the phase coherence between density on the upper and lower electronic surfaces due to the many uncorrelated collisions of the hot carriers with the adsorbate-substrate complex. This Gaussian random process can be modelled by a term $\mathbf{W}_2$,

$$\mathbf{W}_2 = \frac{1}{\sqrt{2}}\mathbf{S} \equiv \frac{1}{\sqrt{2}}\begin{pmatrix} 1 & 0 \\ 0 & -1 \end{pmatrix} , \qquad (9)$$

and an (ultrafast) dephasing rate γ_2. Again it is easy to verify that

$$\frac{\partial}{\partial t}\begin{pmatrix} \rho_{\mathrm{e}} & \rho_{\mathrm{i}} \\ \rho_{\mathrm{i}}^{+} & \rho_{\mathrm{g}} \end{pmatrix}_{\mathrm{diss},2} = \gamma_2 \begin{pmatrix} 0 & -\rho_{\mathrm{i}} \\ -\rho_{\mathrm{i}}^{+} & 0 \end{pmatrix} . \qquad (10)$$

Eq. (10) lends itself to the obvious interpretation that phase coherencies between the negative ion resonance and the neutral state are destroyed with a rate γ_2, but that otherwise no norm or energy flow occurs.

The third dissipative channel considered concerns the hot-electron mediated *excitation* step. Clearly, norm and energy will now be transferred in the direction g→e. An operator $\mathbf{W}_3$,

$$\mathbf{W}_3 = \mathbf{S}_+ \equiv \begin{pmatrix} 0 & 1 \\ 0 & 0 \end{pmatrix} , \qquad (11)$$

is easily seen to achieve this. From Eqs. (3) and (4) we get

$$\frac{\partial}{\partial t}\begin{pmatrix} \rho_{\mathrm{e}} & \rho_{\mathrm{i}} \\ \rho_{\mathrm{i}}^{+} & \rho_{\mathrm{g}} \end{pmatrix}_{\mathrm{diss},3} = \gamma_3 \begin{pmatrix} \rho_{\mathrm{g}} & -\tfrac{1}{2}\rho_{\mathrm{i}} \\ -\tfrac{1}{2}\rho_{\mathrm{i}}^{+} & -\rho_{\mathrm{g}} \end{pmatrix} , \qquad (12)$$

which supports the statement on mass transport just given.

A critical point concerns the choice of the excita-

tion rate, γ_3. In the case of DIMET, where one has a thermal, hot electron ensemble characterized by a sharply peaked temperature profile $T_e(t)$, the *principle of detailed balance* relates γ_3 to γ_1,

$$\gamma_3(z,t)=\gamma_1(z)\exp\{-\beta_e(t)[V_e(z)-V_g(z)]\}. \quad (13)$$

Here, the exponential term $\exp[-\beta_e(V_e-V_g)]\equiv f(E=V_e-V_g)$ reflects the Boltzmann energy distribution $f(E)$ of hot carriers with translational energy E, and

$$\beta_e(T)=\frac{1}{k_B T_e(t)}. \quad (14)$$

Eq. (13) reflects the assumption that the electronic transition is impulsive on the timescale of nuclear motion. The function T_e can, in principle, be obtained from the solution of coupled heat transport equations. Here we use a model function suggested by Heinz and co-workers [7]

$$T_e(t)=T_{e0}\frac{\exp(-t/\tau_e)}{\exp(-t/\tau_p)+1}, \quad (15)$$

where the parameters T_{e0}, τ_p and τ_e are related to the maximum electronic temperature, the laser pulse width and a response time of the metal electrons. From Eq. (13) we note that γ_3 is not only t-dependent, but, through the difference $V_e(z)-V_g(z)$ and a probable dependence of γ_1 on z, also z-dependent. This means that γ_3 also becomes a spatially dependent operator and Eq. (12) has to be modified accordingly. In this study we neglect all z-dependencies on γ_3, i.e. we work with a fixed energy difference $\Delta V=0.1$ hartree (which is the difference $V_e(z)-V_g(z)$ at $z=z_0$), and with a constant γ_1.

In the case of DIET experiments, the electronic temperature is constantly low and the excitations in the soldi are permanently held in a non-equilibrium state. Thus a different distribution function $f(E=V_e-V_g)$ must be employed in Eq. (13). Weik et al. [8] have shown that $f(E)$ follows a power law in E and that relevant parameters can be obtained from laser and substrate characteristics. Based on their arguments, we estimate $f(\Delta V)=0.05$. In contrast to the DIMET experiment, the hot electron concentrations are low for DIET, and excitation becomes a statistically rare event. Therefore we model the DIET excitation rate by a narrow plateau function with height $\gamma_3=0.05\,\gamma_1$, and choose the width of the plateau function to be in the order of 1 fs, the approximate time it takes a 3 eV electron to travel the distance from the surface to the adsorbate molecule.

No other dissipative channels, such as vibrational relaxation and vibrational dephasing are considered. These processes are characterized by timescales of several ps, whereas the events studied below take place on the fs timescale. With the same argument we also neglect the gradual heating of the substrate phonons in the DIMET experiment (though effects of different initial lattice temperatures will be addressed.

The Liouville–von Neumann equation (3) is solved numerically along the lines of previous work [15]. In short, (1) all operators are represented on an evenly spaced spatial grid, (2) all commutators or anticommutators in Eq. (3) are evaluated locally, i.e. in a representation in which the corresponding operators are diagonal. (3) Further, the time propagation is done in small time segments Δt, and a Newton polynomial expansion of the propagator $\exp(-iLt/\hbar)$ is used. (L is the Liouvillian superoperator which gives, when acting on ρ, the right-hand side of Eq. (3)). The optimum sampling points in the complex plane to represent the (due to dissipation) complex eigenvalues of the Liouvillian, are obtained through Schwartz–Christoffel conformal mapping. The reader is referred to Ref. [15] for further details.

The results below refer to the use of 16 sampling points at a time step of $\Delta t=40$ atomic time units (≈ 1 fs). A spatial grid of 256 points with spacing $\Delta=0.04$ a_0, starting at $z_0=0.84$ a_0 was employed. Absorbing boundaries are used at the right-hand side of the grid to avoid reflection and/or reappearance of particle density associated with the use of a finite grid. Initial densities are computed either according to

$$\begin{pmatrix}\rho_e(0) & \rho_i(0)\\ \rho_i^+(0) & \rho_g(0)\end{pmatrix}=\begin{pmatrix}\rho(0) & 0\\ 0 & 0\end{pmatrix} \quad (16)$$

or

$$\begin{pmatrix}\rho_e(0) & \rho_i(0)\\ \rho_i^+(0) & \rho_g(0)\end{pmatrix}=\begin{pmatrix}0 & 0\\ 0 & \rho(0)\end{pmatrix}. \quad (17)$$

Eq. (16) has been used in examples where only the deexcitation dynamics were of interest, and Eq. (17) if the excitation process was explicitly considered. In

both cases $\rho(0)$ is computed according to

$$\rho(0)=\sum_j g_j|\psi_j\rangle\langle\psi_j| \tag{18}$$

as a Boltzmann-weighted sum over products of bound state vibrational functions $|\psi_j\rangle$ and their complex-conjugates. the $\{\psi_j\}$ are numerically obtained from

$$\boldsymbol{H}_g\psi_j=\epsilon_j\psi_j\,, \tag{19}$$

and the Boltzmann weights $\{g_j\}$ are

$$g_j=\frac{\exp(-\beta_s\epsilon_j)}{\mathrm{tr}[\exp(-\beta_s\boldsymbol{H}_g)]}\,, \tag{20}$$

where the terms $\beta_s\equiv 1/k_B T_s$ reflect the dependence of $\rho(0)$ on the surface temperature, T_s.

3. Results and discussion

To keep things as simple and pedagogic as possible, we first consider an academic example, where (i) it is assumed that at $t=0$ the density is given by Eq. (16) and where (ii) an unrealistically small deexcitation rate $\gamma_1=1/1000$ atu is used (corresponding to a negative ion resonance lifetime of $\tau_R=1/\gamma_1\sim 25$ fs). The initial condition is equivalent to the one employed by Gadzuk et al. [9]. Further, no non-adiabatic coupling ($A=0$ in Eq. (6)), no direct or indirect excitation ($\mu_{eg}=0$ in Eq. (6), $\gamma_3=0$ in Eq. (12)), and no electronic dephasing ($\gamma_2=0$ in Eq. (10)) has been assumed.

For the case $T_s=0$ K, Fig. 1 shows some characteristics of the time evolution of the initial density (16). Since in density matrix theory the expectation value of any operator $\boldsymbol{A}$ is obtained from

$$\langle\boldsymbol{A}\rangle=\mathrm{tr}[\boldsymbol{A}\rho]\,, \tag{21}$$

most of the computed quantities are related to trace operations. In Fig. 1a the norms of the excited and ground states, $N_e=\mathrm{tr}[\rho_e(t)]$ and $N_g=\mathrm{tr}[\rho_g(t)]$, are displayed as functions of time. A third curve shows the quantity

$$C_e(t)=\mathrm{tr}[\rho_e(0)\rho_e(t)]\,, \tag{22}$$

related to a correlation function for the density on the upper surface. From Fig. 1a we note that the integrated density on V_e decreases exponentially (with the rate γ_1), as it should. At the same time the norm

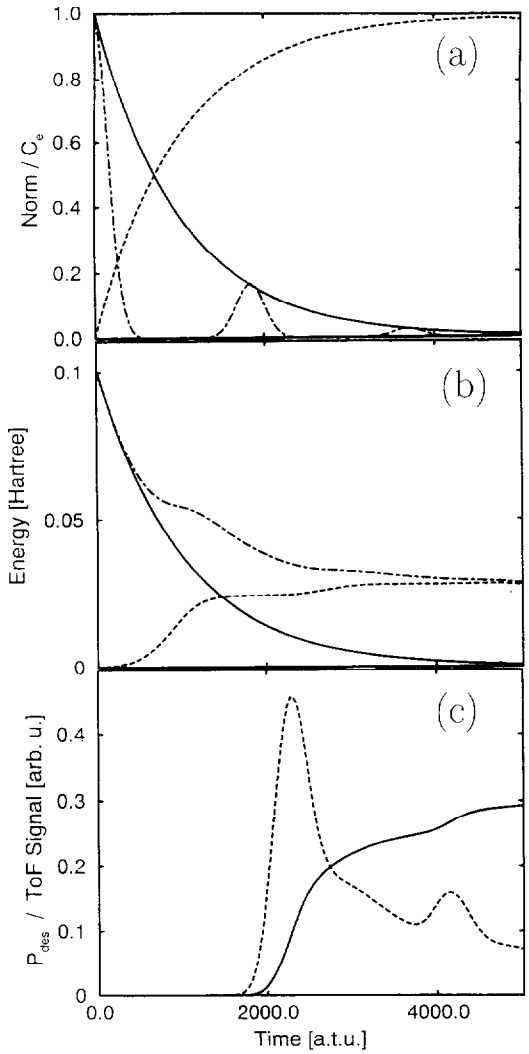

Fig. 1. Several quantities characterizing the desorption dynamics of NO/Pt(111) if only the deexcitation process (with rate $\gamma_1=1/1000$ atu) is considered. (a) Norm of density on V_e (——) and V_g (- - -), correlation function C_e (-·-·-); (b) energy-related quantities $\mathrm{tr}[\boldsymbol{H}_e\rho_e]$ (——), $\mathrm{tr}[\boldsymbol{H}_g\rho_g]$ (- - -), and the sum of the two (-·-·-); (c) desorption probability (Eq. (23)) (——) and density-time-of-flight signal (Eq. (24)) (- - -).

on V_g increases accordingly. The quantity $C_e(t)$ reflects the damped, dissipative oscillation of ρ_e on V_e. Fig. 1b gives energy-like quantities, namely $\mathrm{tr}[\boldsymbol{H}_l\rho_l]$ (l=e, g) and the sum of the two, which is a measure for the total energy contained in the 'system'. Clearly the mass transport causes an energy transfer in the direction e→g. We note that energy is absorbed by

the 'bath', as expected for an irreversible dissipative process.

In Fig. 1c, two quantities of major experimental relevance are shown as a function of time. The first curve gives the desorption probability $P_{\mathrm{des}}(t)$, derived from a partial trace structure over the density matrix in configuration space representation

$$P_{\mathrm{des}}(t)=1-\sum_{i}^{N_{\mathrm{d}}}\rho_{\mathrm{g}}(z_i,z_i)\,. \tag{23}$$

Here, $z_i=z_0+(i-1)\Delta$ are the grid points, and N_{d} is a grid point separating 'trapped' from 'desorbed' density (we took $z_{\mathrm{d}}=z_0+(N_{\mathrm{d}}-1)\Delta=4.9\,a_0$). In Eq. (23) only the ground state density enters, since for the present system exclusively desorption of neutrals is important. The second curve in Fig. 1c shows a 'density time-of-flight spectrum', taken as the diagonal element of the density matrix block ρ_{g} at the point z_{d} separating reactants from products

$$I(t)=\rho_{\mathrm{g}}(z_{\mathrm{d}},z_{\mathrm{d}})\,. \tag{24}$$

According to Fig. 1c, $P_{\mathrm{des}}(t)$ reaches an almost constant value of 0.3 after around 5000 atu ($\approx$125 fs), and correlates with the integrated signal of $I(t)$. The peak structure observed for $I(t)$ (which will vanish for realistically short lifetimes τ_{R}) resembles the oscillatory nature of the density on V_{e}. In the sense of Antoniewicz' model only those parts of the density have a significant chance to desorb, which – after moving towards the surface – deexcite in the strongly repulsive regions of V_{g}. In an oscillating system, these favourable conditions repeat periodically. It is straightforward to derive also a 'flux time-of-flight spectrum', and/or to perform a kinetic energy analysis of the desorbing particles. For reasons of compactness, however, this task will be postponed to a forthcoming paper [16].

Instead, we show in some more detail how the density evolves in configuration and phase space. The evolution of the excited state density has already been anticipated in Fig. 1b in the form of the quantity $C_{\mathrm{e}}(t)$. The time evolution of the ground state density ρ_{g} on V_{g} is demonstrated in Fig. 2 through the quantities $\rho_{\mathrm{g}}(z,z)$, shown at three different times, $t=1200$, $t=2400$ and $t=4800$ atu ($\approx$30, 60 and 90 fs). The diagonal elements of the density matrix in configuration space representation give the particle density at the respective space points. Hence the curves shown

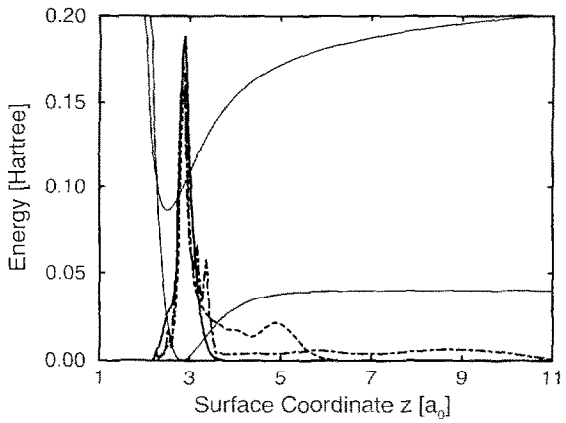

Fig. 2. Diagonals of the ground state density matrix in configuration space (arb. units) for the same process as in Fig. 1: $\rho_{\mathrm{g}}(z,z)$ for $t=1200$ atu (——), $\rho_{\mathrm{g}}(z,z)$ for $t=2400$ atu (- - -), $\rho_{\mathrm{g}}(z,z)$ for $t=4800$ atu (-·-·-); also shown are the ground and excited state potentials.

in Fig. 2 are analogous to the snapshots frequently shown in wave packet dynamics. We note that (i) (neutral) particle density increases with time on the ground state surface and that (ii) the ground state density splits at later times into a trapped and a desorbing part. More detailed information is provided by the Wigner distribution function in phase space [17],

$$w_l(z,p_z)=\frac{1}{2\pi}\int \mathrm{d}y\exp(\mathrm{i}p_z y)\rho_l(z-\tfrac{1}{2}y,z+\tfrac{1}{2})\,, \tag{25}$$

(l=e, g) which is the quantum counterpart to a classical probability $\tilde{w}(z,p_z)$ to find a particle at phase space point (z,p_z). In Fig. 3a we show the initial (excited state) Wigner distribution $w_{\mathrm{e}}(z,p_z)$ at $t=0$, whereas Fig. 3b gives the ground state distribution $w_{\mathrm{g}}(z,p_z)$ at a later time, $t=2400$ atu. Initially, the Wigner distribution is a Gaussian in phase space, with particle density localized around the ground state potential well and with zero mean momentum. At the later time, when density has been transferred in the direction e→g, a part of this density has been retrapped in the ground state well, another one leaks out towards larger z values. For the desorbing particles, one roughly estimates a mean momentum of $|\langle p_z\rangle|\approx 50$ atomic momentum units, which corresponds to a classical speed of about 2000 m/s or a

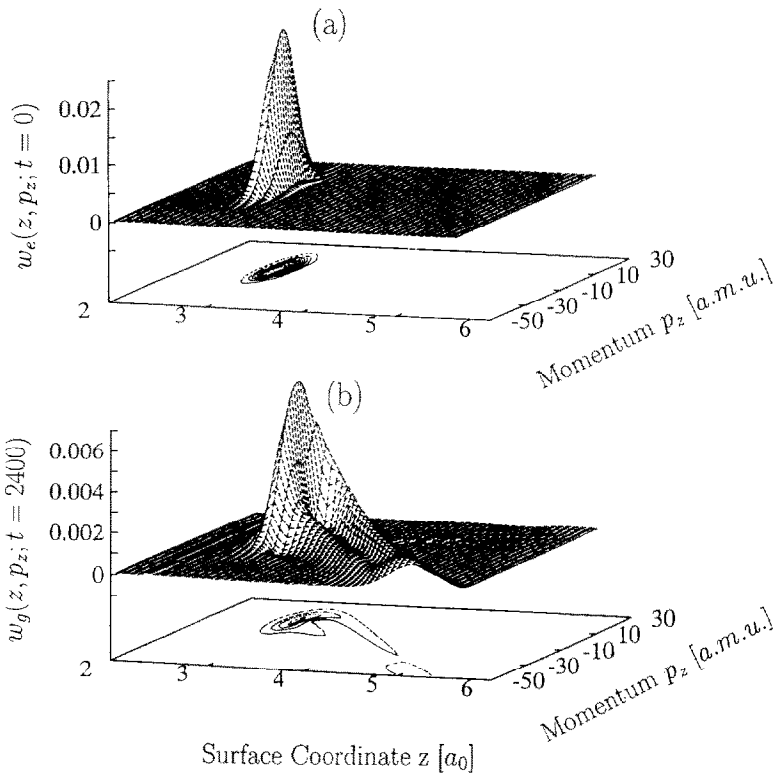

Fig. 3. Wigner distribution functions (Eq. (25)) for the same process as in Figs. 1 and 2: (a) w_e, $t=0$; (b) w_g, $t=2400$ atu. Arbitrary units for the 'z axis'.

temperature of 14000 K! This result, together with the six orders of magnitude overestimation of the experimental desorption probability [6], is a consequence of the artificial assumptions made in our pedagogical (i.e. 'large effects') example, namely the use of an unrealistically large resonance lifetime and the neglect of the excitation process.

Concerning the first point, Gadzuk [9] has clearly shown that $P_{\mathrm{des}} \equiv \lim_{t\to\infty} P_{\mathrm{des}}(t)$ is a strongly decreasing function with decreasing resonance lifetime, τ_{R}. This effect can also be demonstrated in density matrix theory. Within the deexcitation-only scenario exercised above, we obtain for three different quenching rates $\gamma_1 = 1/1000$ atu ($\tau_{\mathrm{R}} \approx 25$ fs), $\gamma_1 = 5/1000$ atu ($\tau_{\mathrm{R}} \approx 5$ fs), and $\gamma_1 = 1/100$ atu ($\tau_{\mathrm{R}} \approx 2.5$ fs), the desorption probabilities $P_{\mathrm{des}}(t=5000 \text{ atu}) = 0.29$, 5.7×10^{-2} and 5.1×10^{-3}, respectively. Even more drastic reductions are observed after explicit inclusion of the excitation process.

Before doing so, however, we will first consider the effects of surface temperature T_{s}, and the role of electronic dephasing and non-adiabatic couplings between V_{g} and V_{e} within the deexcitation-only model. In Fig. 4 the desorption probability is shown as a function of time for the case $\gamma_1 = 5/1000$ atu ($\tau_{\mathrm{R}} \approx 5$s) for four different situations. The first curve (solid) is a reference function, obtained for surface temperature $T_{\mathrm{s}}=0$ K, dephasing rate $\gamma_2=0$ and non-adiabatic coupling strength $A=0$. Here, $P_{\mathrm{des}}(t)$ saturates at $P_{\mathrm{des}} \approx 0.06$, the value given in the last paragraph. The second curve (dashed), shows the result for the same parameters, except $T_{\mathrm{s}} = 500$ K. We note that the desorption probability is somewhat ($\approx 5\%$) enhanced. This is easily understood with the help of Antoniewicz' model. The thermal initial density, given by Eqs. (18) and (20) is broader in configuration space than the $T_{\mathrm{s}}=0$ K density. (Of course, it is also broader in momentum space.) Thus part of

the density has to travel only a short distance towards the surface plane to reach highly repulsive regions on V_g and desorb. This can be achieved even within an ultrashort resonance lifetime. Though not shown here, one also observes a broadening of the density-time-of-flight spectrum in the high-T_s case.

From Fig. 4 it is further seen that in contrast to surface temperature, electronic dephasing and non-adiabatic couplings do not play any significant role. Curves 3 and 4 in Fig. 4, in which electronic dephasing (with a rate $\gamma_2 = 5/1000$ atu) or non-adiabatic coupling (with parameters $A = 0.05$ eV and $b = (0.1\ a_0)^2$) were included, respectively, are almost identical to the reference case. Variation of these parameters in reasonable ranges did not change the results either. This is easily rationalized. The individual non-adiabatic coupling between V_g and V_e is much too weak to be relevant on the short timescales considered here. (The couplings of V_e to the continuum of metal excited states, however, sum up to give the ultrafast process, which is modelled by the the dissipative term (8)). Further, electronic dephasing will be important for phase sensitive quantities such as correlation functions and hence, absorption spectra. They will be less important for solely density-dependent quantities, such as P_{des} (Eq. (23)) or the time-of-flight signals (Eq. (24)).

Finally, the excitation process was considered in some detail and the initial density Eq. (17) used rather than (16). For the DIMET process, Eq. (13) is employed to relate the excitation rate γ_3 to the quenching rate γ_1, which is again chosen to be $\gamma_1 = 5/1000$ atu. The electronic temperature profile is given by the peak function (15) with a maximum temperature $T_{e,max} \approx 4200$ K reached after ≈ 50 fs. The resulting transition rate $\gamma_3(t)$ is also a peak function with a maximum $\gamma_{3,max} \approx 2 \times 10^{-6}$ reached after ≈ 50 fs and a width at half maximum of about 100 fs. We do not display $T_e(t)$ or $\gamma_3(t)$ here, but rather show the response of the system in Fig. 5 in the form of the norm $N_e(t)$ on the upper surface (solid curve), and the desorption probability $P_{des}(t)$ (dashed curve). It is interesting to note that N_e goes through a maximum but never becomes large in the DIMET experiment, the maximum value being $N_{e,max} \approx 5 \times 10^{-4}$. The second observation is that the desorption probability drops once more by more than two orders of magnitude (relative to the completely inverted initial condition (16)), and is in the order of magnitude of $N_{e,max}$: $P_{des}(t = 5000\ \text{atu}) = 2.4 \times 10^{-4}$. This value is expected to further decrease for shorter resonance lifetimes.

To simulate the DIET experiment a one-time step, narrow-plateau function is chosen for γ_3 as described

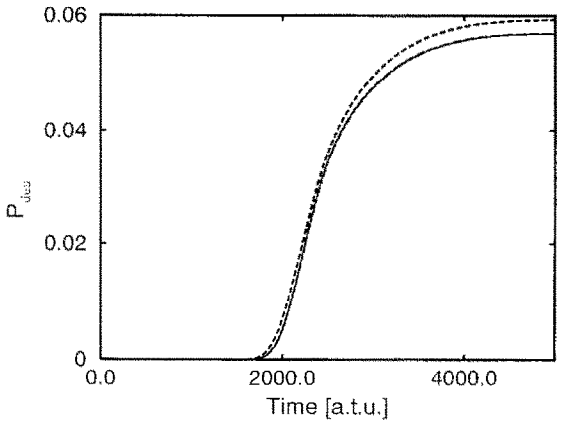

Fig. 4. Desorption probability for the same process as in Figs. 1–3 for the 'reference case' (——) and the 'enhanced surface temperature case' (- - -). Hardly visible (since coinciding with curve 1) are the 'electronic dephasing curve' (-·-·-), and the 'non-adiabatic coupling curve') (– – –).

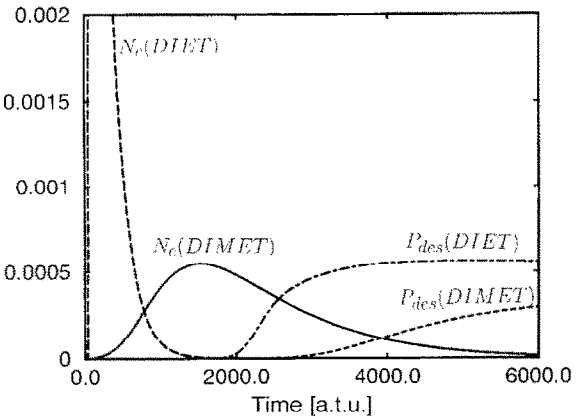

Fig. 5. Quantities characterizing the desorption of NO from Pt(111) if the excitation step is explicitly considered ($\gamma_1 = 5/1000$ atu). Simulated are a DIMET experiment (Eqs. (13) and (15), with $T_{e0} = 5000$ K, $\tau_e = 250$ fs, $\tau_p = 10$ fs) and a DIET experiment (narrow plateau excitation after $t = 1$ fs with a rate $\gamma_3 = 0.05\ \gamma_1$). Shown are the excited state populations N_e(DIMET) (——) and N_e(DIET) (which reaches a maximum of $\approx 9 \times 10^{-3}$) (- - -), along with the desorption probabilities P_{des}(DIMET) (- - -) and P_{des}(DIET) (-·-·-).

above. In Fig. 5 we also give $N_e(t)$ (long-dashed) and $P_{des}(t)$ (dot-dashed) for the DIET case. Now, $N_e(t)$ suddenly peaks at an early excitation time (chosen to be 1 fs) reaching a maximum of 9×10^{-3}. Then the negative ion resonance decays exponentially and the desorption of particles begins after about 2500 atu (70 fs), saturating at a value of $P_{des}\approx 5.5\times10^{-4}$. The fact that the asymptotic desorption probability is lower in this particular DIMET example than in the particular DIET example should not be generalized; only if apart from the pulse width identical laser characteristics (fluence, frequency) were usedf, both calculations were comparable. In the simplified treatment given here, however, this is not the case. In fact, in both cases the population on the excited surface is quite low, but the DIMET resonance population is a much smoother, low-valued function in time than the DIET population. Given the fact that in the present example the ratio of the maximum populations is $N_{e,max}(\mathrm{DIET})/N_{e,max}(\mathrm{DIMET})\approx 20$, it is remarkable that the final desorption probabilities differ only by a factor of ≈ 2. This may be a theoretical rationalization for the experimental observation that (under comparable conditions) multiple excitations lead to larger desorption yields than (individual 'effective') single-excitations. Clearly, this point must be clarified further by taking laser and material characteristics explicitly into account.

4. Conclusions

In conclusion, we have shown that a realistic treatment of a complex process such as laser-induced hot-electron mediated desorption of small molecules from metals is possible within the quantum mechanical framework of the Liouville–von Neumann formalism. The numerical evaluation of the underlying equations allows not only the use of realistic potentials, but also to simulate different dissipative processes and special excitation limits. Desorption probabilities of the right order of magnitude and reasonable time-of-flight spectra are obtained. We gain insight into details of mass and energy flow and can study surface temperature effects. The present treatment suffers from the use of empirical (dissipative) parameters. In many cases, however, these are well known experimentally, for others it is hoped that a microscopic theory can provide them. More details of the present work, along with the computation of other experimentally relevant quantities (such as flux time-of-flight spectra) and a detailed inclusion of laser characteristics during excitation will be published elsewhere [16].

Acknowledgement

It is a pleasure to thank Allon Bartana for providing his computer program to solve the Liouville–von Neumann equation for ions in solution. Fruitful discussions with Allon Bartana, Jörn Manz, Eckart Hasselbrink and Martin Wolf are gratefully acknowledged. The Fritz Haber Research Centers is supported by the Minerva Gesellschaft für die Forschung, GmbH München, Germany. PS thanks the Deutsche Forschungsgemeinschaft (Sfb 337) for a travel grant.

References

[1] D. Menzel and R. Gomer, J. Chem. Phys. 41 (1964) 3311; P.A. Redhead, Can. J. Phys. 42 (1980) 886.
[2] P.R. Antoniewicz, Phys. Rev. B 21 (1980) 3811.
[3] Z.W. Gortel, R. Teshima and H.J. Kreuzer, Phys. Rev. B 37 (1988) 3183.
[4] J.C. Polanyi and H. Rieley, in: Dynamics of gas–surface interactions, eds. C.T. Rettner and M.N.R. Ashfold (Royal Society of Chemistry, London, 1991).
[5] N.H. Tolk, M.N. Traum, J.C. Tully and T.E. Madey, eds., DIET I: Desorption induced by electronic transitions, Workshops Proceedings (Springer, Berlin, 1983);
W. Brenig and D. Menzel, eds., DIET II, Workshop Proceedings (Springer, Berlin, 1985);
R.H. Stulen and M.L. Knotek, eds., DIET III, Workshop Proceedings (Springer, Berlin, 1988);
G. Betz and P. Varga, eds., DIET IV, Workshop Proceedings (Springer, Berlin, 1988);
A.R. Burns, E.B. Stechel and D.R. Jennison, eds., DIET V, Workshop Proceedings (Springer, Berlin, 1993).
[6] S.A. Buntin, L.J. Richter, R.R. Cavanagh and D.S. King, Phys. Rev. Letters 61 (1988) 1321.
[7] J.A. Prybyla, T.F. Heinz, J.A. Misewich, M.M.T. Loy and J.H. Glowina, Phys. Rev. Letters 64 (1990) 1537.
[8] F. Weik, A. de Meijere and E. Hasselbrink, J. Chem. Phys. 99 (1993) 682.
[9] J.W. Gadzuk, L.J. Richter, S.A. Buntin, D.S. King and R.R. Cavanagh, Surface Sci. 235 (1990) 317;
J.W. Gadzuk, Phys. Rev. B 44 (1991) 13.
[10] S. Harris and S. Holloway, to be published.

[11] R. Alicki and K. Landi, Quantum dynamical semigroups and applications (Springer, Berlin, 1987).
[12] C. Daniel, R. de Vivie-Riedle, M.-C. Heitz, J. Manz and P. Saalfrank, submitted for publication.
[13] U. Banin, A. Bartana, S. Ruhman and R. Kosloff, J. Chem. Phys., in press.
[14] G. Lindblad, Commun. Math. Phys. 33 (1973) 305.
[15] M. Berman and R. Kosloff, Comp. Phys. Commun. 63 (1991) 1;
M. Berman, R. Kosloff and H. Tal-Ezer, J. Phys. A 25 (1992) 1283.
[16] P. Saalfrank and R. Kosloff, to be published.
[17] E.P. Wigner, Phys. Rev. 40 (1932) 749;
M. Hillery, R.F. O'Connell, M.O. Scully and E.P. Wigner, Phys. Rept. 106 (1984) 121.